Photoacid Behavior versus Proton-Coupled Electron Transfer in Phenol–$[Ru(bpy)_3]^{2+}$ Dyads

Journal:	*The Journal of Physical Chemistry*
Manuscript ID:	jp-2013-02567m.R1
Manuscript Type:	Article
Date Submitted by the Author:	27-May-2013
Complete List of Authors:	Kuss-Petermann, Martin; Georg-August-Universität, Institut für Anorganische Chemie Wenger, Oliver; University of Basel, Department of Chemistry

Photoacid Behavior versus Proton-Coupled Electron Transfer in Phenol–$Ru(bpy)_3^{2+}$ Dyads

Martin Kuss-Petermann[†] *and Oliver S. Wenger**[‡]

[†]*Institut für Anorganische Chemie, Georg-August-Universität Göttingen, Tammannstraße 4, D-37077 Göttingen, Germany.*

[‡]*Departement für Chemie, Universität Basel, Spitalstrasse 51, CH-4065 Basel, Switzerland.*

oliver.wenger@unibas.ch

ABSTRACT

Two dyads comprised of a $Ru(bpy)_3^{2+}$ (bpy = 2,2'-bipyridine) photosensitizer and a covalently attached phenol were synthesized and investigated. In the shorter dyad (Ru–PhOH) the ruthenium complex and the phenol are attached directly to each other whereas in the longer dyad there is a *p*-xylene spacer in between (Ru–xy–PhOH). Electrochemical investigations indicate that intramolecular electron transfer (ET) from phenol to the photoexcited metal complex is endergonic by more than 0.3 eV in both dyads, explaining the absence of any ^{3}MLCT excited-state quenching by the phenols in pure CH_3CN and CH_2Cl_2. When adding pyridine to a CH_2Cl_2 solution, significant excited-state quenching can be observed for both dyads, but the bimolecular quenching rate constants differ by two orders of magnitude between Ru–PhOH and Ru–xy–PhOH. Transient absorption spectroscopy shows that in presence of pyridine both dyads react to photoproducts containing Ru(II) and phenolate. The activation energies associated with the photoreactions in the two dyads differ by one order of magnitude, and this might suggest that the formation of identical photoproducts proceeds through fundamentally different reaction pathways in Ru-PhOH and Ru-xy-PhOH. For Ru-PhOH direct proton release from the photoexcited dyad is a plausible reaction pathway. For Ru-xy-PhOH a sequence of a photoinduced proton-coupled electron transfer (PCET) followed by an intramolecular (thermal) electron transfer in the reverse direction is a plausible reaction pathway; this two-step process involves a reaction intermediate containing Ru(I) and phenoxyl radical which reacts very rapidly to Ru(II) and phenolate. Thermal back reactions to restore the initial starting materials occur on a 30 μs – 50 μs timescale in both dyads, i. e., due to proton release the photoproducts are very long lived. These back-reactions exhibit inverse H/D kinetic isotope effects of 0.7±0.1 (Ru–PhOH) and 0.6±0.1 (Ru–xy–PhOH) at room temperature.

KEYWORDS

Proton-coupled electron transfer, phenols, ruthenium, photochemistry, photoacid, electron tunneling

INTRODUCTION

Proton-coupled electron transfer (PCET) is an elementary reaction in many enzymes, and it is of key importance for example for water oxidation or carbon dioxide reduction hence it seems desirable to understand PCET at the most fundamental level.[1, 2] Phenols are well suited PCET reactants for mechanistic studies because the acidity of their OH group and their oxidation potential are strongly interrelated.[3, 4] There have been numerous studies of PCET with phenols, focusing on various aspects such as the driving-force dependence of reaction rates and mechanisms,[5-8] the importance of hydrogen-bonding,[9-21] proton transfer distance,[22, 23] and pH of the surrounding medium.[15, 24-27] The importance of the separation between the redox-active and the acidic/basic reaction sites has also been studied in suitable models.[28, 29] However, the influence of the electron donor-acceptor distance on PCET rates and mechanisms is yet poorly explored,[30, 31] unlike the distance dependence of "simple" (= not proton-coupled) electron transfer.[32-37]

Scheme 1. (a) The P680 / TyrZ / His-190 bidirectional PCET reaction triple of photosystem II; (b) functional model compounds investigated in this work (n = 0, 1).

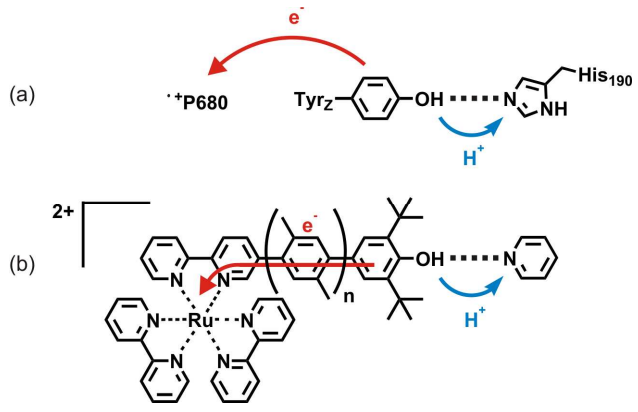

PCET reactivity in model systems can be induced chemically,[5, 14, 23] electrochemically,[8, 38, 39] or photochemically.[15, 17, 21, 40-44] Our group recently reported on phototriggered bimolecular PCET between phenols and Ru(2,2'-bipyrazine)$_3^{2+}$ or rhenium(I) tricarbonyl complexes.[45-47] Building on this work we investigated the influence of electron donor-acceptor distance on the PCET chemistry of covalent rhenium(I)-phenol dyads in CH_3CN/H_2O mixtures.[30] In this paper we report on analogous Ru(bpy)$_3^{2+}$–phenol dyads and their photochemistry in CH_2Cl_2/pyridine solution. Our system may be regarded as a functional model for the P680 / TyrZ / His-190 reaction triple of photosystem II (Scheme 1):[48] The phenol plays the role of the combined electron/proton donor (TyrZ), the photoexcited Ru(bpy)$_3^{2+}$ mimicks the function of P680, and the pyridine acts as a base like His-190. While similar functional models have been reported previously,[21, 25, 44, 49-53] the influence of the distance between the phenolic electron donor and the electron acceptor on the overall PCET chemistry is yet little explored. In one of our dyads the phenol is attached directly to the Ru(bpy)$_3^{2+}$ complex (Ru–PhOH), whereas in the other there is a *p*-xylene spacer in between (Ru–xy–PhOH).

RESULTS AND DISCUSSION

UV-Vis spectroscopy and cyclic voltammetry. Figure 1 shows the UV-Vis absorption spectrum of Ru–PhOH and Ru–xy–PhOH at $3 \cdot 10^{-5}$ M concentration in CH_2Cl_2 at 295 K. For both compounds the usual absorptions of the Ru(bpy)$_3^{2+}$ complex, namely an MLCT (metal-to-ligand charge transfer) band centered around 450 nm and a bpy-localized π-π* transition near 300 nm are observed. The shorter dyad exhibits an additional band near 380 nm which had been observed previously in a closely related rhenium(I) complex with a pendant phenol.[30]

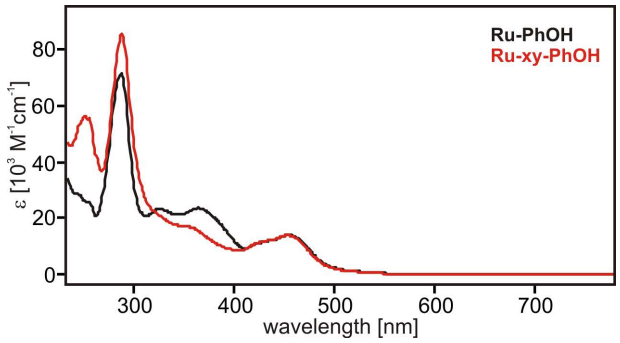

Figure 1. UV-Vis absorption spectra of the two dyads in CH_2Cl_2 at 295 K.

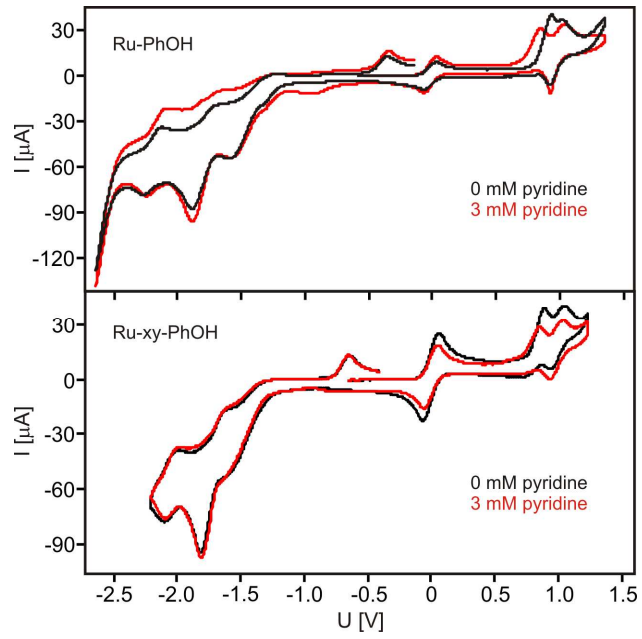

Figure 2. Cyclic voltammograms of Ru–PhOH (upper half) and Ru–xy–PhOH (lower half) in pure CH_2Cl_2 (black traces) and in CH_2Cl_2 with 3 mM pyridine (red traces). The supporting electrolyte was 0.1 M $TBAPF_6$, the voltage scan rate was 100 mV/s.

The reduction potentials of the individual electrochemically active components of Ru–PhOH and Ru–xy–PhOH were extracted from the data in Figure 2. The cyclic voltammograms were recorded in de-oxygenated and freshly distilled CH_2Cl_2 (black traces) in presence of 0.1 M $TBAPF_6$ (TBA = tetra-*n*-butylammonium). Ferrocene (Fc) was added for internal voltage calibration, manifesting in the reversible waves at 0.0 V. Near 1.0 V vs. Fc^+/Fc one detects two oxidation processes in both dyads: One

of them is reversible and is attributed to the $Ru(bpy)_3^{3+}/Ru(bpy)_3^{2+}$ couple. The other is irreversible and is assigned to the $PhOH^+/PhOH$ couple. The values in Table 1 are half-wave potentials; for the irreversible phenol oxidation processes we used the inflection point in the rising part of the observable wave as an approximate value; we did not detect any significant voltage scan rate dependence for any of these potentials. As seen from Table 1, the $Ru(bpy)_3^{2+}$ oxidation potentials are very close to 1.0 V vs. Fc^+/Fc, while phenol oxidation occurs near 0.9 V vs. Fc^+/Fc, both in line with literature values.[3, 4, 54] The irreversibility of the phenol oxidation is commonly attributed to proton loss to bulk solution. [3, 4, 9-11] On the reductive side of the voltage sweeps we detect prominent waves which can be attributed to reduction of the bpy ligands with up to three electrons.[54] The subsequent oxidative sweep between -2.5 V vs. Fc^+/Fc and 0 V vs. Fc^+/Fc reveals an irreversible oxidation at -0.40 V vs. Fc^+/Fc for Ru–PhOH and at -0.70 V vs. Fc^+/Fc for Ru–xy–PhOH. The respective waves only appear after an initial oxidative sweep to potentials more positive than 0.8 V vs. Fc^+/Fc, and consequently we attribute these waves to oxidation of phenolate to phenoxyl radical. The phenolate is generated in the course of phenol oxidation as mentioned above.

Table 1. Reduction potentials of the individual electrochemically active components of the two dyads in CH_2Cl_2.

	E(bpy/bpy$^-$)	E(PhO$^{\cdot}$/PhO$^-$)	E(PhOH$^+$/PhOH)	E(Ru^{III}/Ru^{II})	ΔG_{ET}^0
Ru-PhOH	-1.77	-0.40	0.89	0.99	0.34 eV
Ru-xy-PhOH	-1.72	-0.70	0.83	1.00	0.30 eV

All potentials are reported in V vs. Fc^+/Fc, the data was extracted from the voltammograms in Figure 2. The supporting electrolyte was 0.1 M $TBAPF_6$.

Interestingly, the potential for the $PhOH^+/PhOH$ couple is nearly same in Ru–PhOH and Ru–xy–PhOH (0.89 / 0.83 V vs. Fc^+/Fc) whereas phenolate oxidation is easier by 300 mV in the longer dyad. This likely reflects the resonance stabilization of the phenolate in deprotonated Ru–PhOH through

delocalization of the negative charge from the O-atom towards the N-atom of bpy (Scheme 2).[55] In principle one can draw an analogous resonance structure for the bpy-xy-PhOH ligand of the longer dyad but in that system electronic coupling between bpy and PhOH is weaker, and the respective resonance stabilization is probably less important.

The red traces in Figure 2 are the voltammograms of analogous CH_2Cl_2 solutions containing 3 mM pyridine. One detects a small shift of the phenol oxidation potentials to less positive values compared to pure CH_2Cl_2. For Ru–PhOH the $PhOH^+$/PhOH couple shifts from 0.89 V to 0.80 V vs. Fc^+/Fc, for Ru–xy–PhOH it shifts from 0.83 V to 0.80 V vs. Fc^+/Fc. Because of the small magnitude of this shift it is difficult to extract a clear correlation between phenol oxidation potential and pyridine concentration (Figure S1 of the Supporting Information). All other redox potentials stay essentially unchanged upon pyridine addition.

Scheme 2. Two resonance structures of the deprotonated bpy-PhOH ligand in the Ru-PhOH dyad.

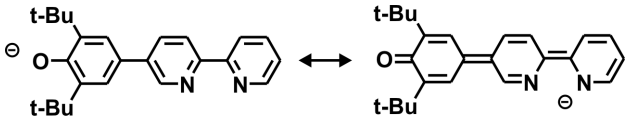

Luminescence and transient absorption spectroscopy. In pure de-oxygenated CH_2Cl_2 solution the ^{3}MLCT excited state of the $Ru(bpy)_3^{2+}$ unit in Ru–PhOH and Ru–xy–PhOH is essentially unquenched, the emission intensities and lifetimes are similar to those of free $Ru(bpy)_3^{2+}$ under identical conditions. By transient absorption spectroscopy one detects the spectral signature of the ^{3}MLCT state of $Ru(bpy)_3^{2+}$ (black traces in Figure 3a/b): A bleach near 450 nm, a positive ΔOD signal around 315 nm, and another bleach near 300 nm.[56] Additionally the spectral signature of the reduced bpy-phenol ligands can be observed as a positive signal around 400 nm ("reduced" when considering the MLCT state as comprised of an oxidized metal center and a reduced ligand). These spectra were recorded by time-averaging over 200 ns after excitation with laser pulses of ~10 ns duration at 532 nm. Evidently, electron transfer (ET)

from phenol to the photoexcited metal complex is not kinetically competitive with inherent ^{3}MLCT deactivation processes under these experimental conditions. The electrochemical data from the previous section are helpful to understand why: Using equation 1 and $E_{ox} = E(PhOH^+/PhOH)$, $E_{red} = E(bpy/bpy^-)$, E_{00} = 2.12 eV and R_{DA} = 7.9 Å for Ru-PhOH / 12.2 Å for Ru-xy-PhOH,[30] we arrive at the conclusion that in CH_2Cl_2 the reaction free energy (ΔG_{ET}^0) associated with electron transfer from phenol to photoexcited $Ru(bpy)_3^{2+}$ is +0.34 eV for Ru–PhOH and +0.30 eV for Ru–xy–PhOH (last column of Table 1).[57] Given the significantly endergonic nature of intramolecular photoinduced electron transfer its kinetic inefficiency is not surprising.

$$\Delta G_{ET}^0 = e \cdot (E_{ox} - E_{red}) - E_{00} - e^2/(4 \cdot \pi \cdot \varepsilon_0 \cdot \varepsilon_s \cdot R_{DA}) \qquad \text{(eq. 1)}$$

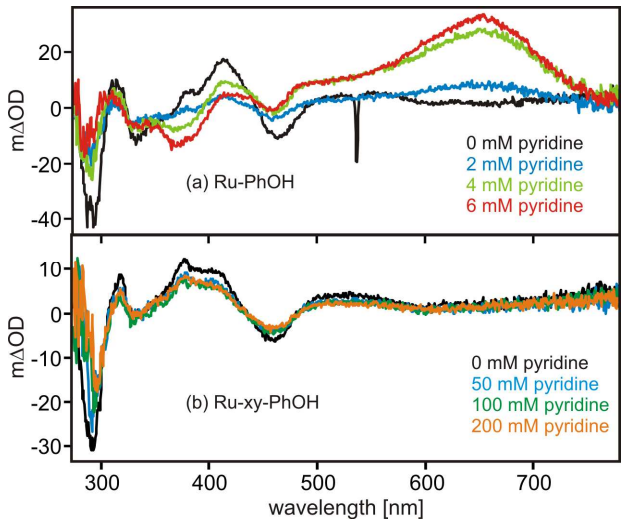

Figure 3. Transient absorption spectra of Ru–PhOH (a) and Ru–xy–PhOH (b) in de-oxygenated CH_2Cl_2 in presence of variable concentrations of pyridine (see inset for color code). The concentration of the dyads was 10^{-5} M in all cases. Excitation occurred with laser pulses of 10 ns width at 532 nm. The spectra are time-averaged over a period of 200 ns starting immediately after the pulse.

When adding pyridine to the CH_2Cl_2 solutions, ^{3}MLCT excited-state quenching is observed in both dyads, manifesting in luminescence intensity decreases and lifetime shortenings (Figure S2 and Figure S3), as well as in the appearance of new signals in the transient absorption spectra: In the Ru–PhOH

dyad pyridine addition leads to the emergence of a broad transient absorption signal in the 480 – 740 nm spectral range (colored traces in Figure 3a) which is obviously due to the formation of a photoproduct. In the Ru-xy-PhOH dyad the photoproducts form much more slowly than in Ru-PhOH (see below) and therefore when time-averaging transient absorption spectra over the first 200 ns after the excitation pulses we mostly observe the spectroscopic signature of the ^{3}MLCT excited state in this case (Figure 3b). Consequently, for identification of the photoproducts it is useful to consider transient absorption spectra that have been recorded with sufficiently long time delays after excitation (using solutions with sufficiently high pyridine concentrations). Such spectra are shown as black traces in Figure 4a (Ru-PhOH, time delay: 2 μs) and in Figure 4c (Ru-xy-PhOH, time delay: 4 μs); the long delays are possible because the photoproducts have lifetimes > 30 μs (see below). The red trace in Figure 4a is a derived spectrum obtained from subtraction of the blue trace in Figure 4b (UV-Vis spectrum of Ru–PhOH in CH_2Cl_2) from the green trace in Figure 4b (UV-Vis spectrum of Ru–PhO$^-$ in CH_2Cl_2; measured after addition of excess TBAOH). There is significant resemblance between the derived (red) and measured (black) spectrum in Figure 4a, suggesting that the observed photoproduct is in fact the ground state of the short dyad in its deprotonated form (Ru-PhO$^-$) with ruthenium in its +II oxidation state. For the longer dyad, we perform a completely analogous analysis: The red trace in Figure 4c is a derived spectrum which is obtained when subtracting the blue trace in Figure 4d (spectrum of Ru-xy-PhOH in CH_2Cl_2) from the green trace in Figure 4d (spectrum of Ru-xy-PhO$^-$). Like for the shorter dyad, there is significant resemblance between experimental (black) and derived (red) spectra in Figure 4c, suggesting that Ru-xy-PhO$^-$ with ruthenium in its +II oxidation state and phenolate are the photoproducts in the longer dyad, too. There are non-negligible red-shifts of some of the experimental band maxima with respect to the calculated maxima in Figure 4a/4c which may have to do with the fact that the experimental transient absorption data were measured in presence of pyridine while the derived spectra rely on data recorded in absence of pyridine. Be that as it may, the similarity of experimental and derived spectra is undeniable. Notably, none of the experimental transient absorption spectra can be reconciled with a Ru(I) photoproduct (for simplicity we use the notation “Ru(I)” to describe a one-

electron reduced complex even though the additional electron is ligand-based) because for this species one would expect intense absorptions at ~380 nm and at ~510 nm combined with a bleach at ~450 nm.[58, 59,60] However the latter two features are absent, and consequently one must observe a Ru(II) species here.

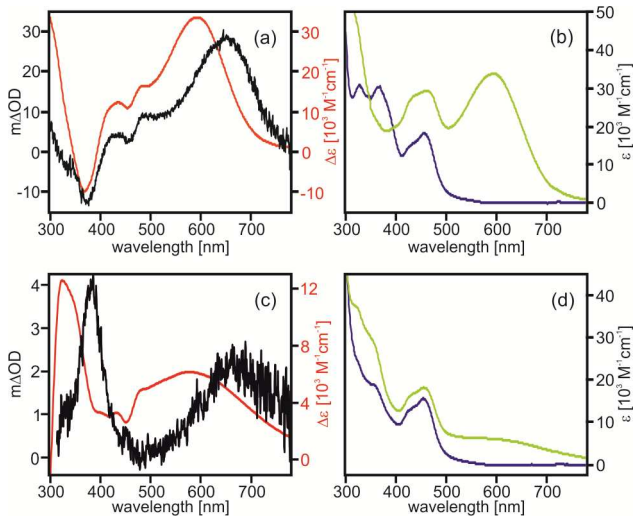

Figure 4 (a) Black trace: transient absorption spectrum measured from Ru–PhOH in CH_2Cl_2 with 6 mM pyridine after excitation at 532 nm with ~10 ns laser pulses; detection occurred by time-averaging over a 200 ns period starting 2 μs after pulsed excitation. Red trace: Spectrum obtained from subtraction of the blue trace in (b) from the green trace in (b). (b) Blue trace: UV-Vis spectrum of Ru–PhOH in CH_2Cl_2; green trace: UV-Vis spectrum of Ru–PhO^- in CH_2Cl_2 (deprotonation occurred using excess TBAOH). (c) Black trace: transient absorption spectrum measured from Ru–xy–PhOH in CH_2Cl_2 with 200 mM pyridine after excitation at 532 nm with ~10 ns laser pulses; detection occurred by time-averaging over a 200 ns period starting 4 μs after pulsed excitation. (d) Blue trace: UV-Vis spectrum of Ru(II)– xy–PhOH in CH_2Cl_2; green trace: UV-Vis spectrum of Ru(II)– xy–PhO^- in CH_2Cl_2 (deprotonation occurred using excess TBAOH).

There are two possible reaction pathways leading to Ru(II) / phenolate photoproducts: (i) simple photoacid behavior, and (ii) a photoinduced PCET reaction in which the phenolic proton is released to

the pyridine base and an electron is transferred from the phenol to the excited $Ru(bpy)_3^{2+}$ complex, followed by rapid (thermal) back-electron transfer from the reduced ruthenium complex to the phenoxyl radical. Such a thermal back-electron transfer is thermodynamically possible because the $Ru(bpy)_3^{2+}$ unit is reduced at substantially more negative potential than the phenoxyl radical; the relevant redox potentials are listed in Table 1. Based on these values the driving-force for the thermal back-electron transfer after initial PCET is ca. -1.37 eV for Ru(I)-PhO· and ca. -1.02 eV for Ru(I)-xy-PhO·. Consequently, if such intermediates are formed, they potentially react very rapidly to Ru(II)-PhO^- and Ru(II)-xy-PhO^-, particularly in view of the high driving-forces and the comparatively short donor-acceptor distances.

For the short Ru-PhOH dyad simple photoacid behavior is a very plausible photochemical reaction pathway for the following reason: Initial MLCT excitation occurs at least partially towards one of the unsubstituted bpy ancillary ligands, and the formal Ru(III) center then increases the acidity of the pendant phenol group. Electrostatically driven changes in acidity and basicity are a common phenomenon for metal complexes with deprotonatable / protonatable ligands,[5, 55, 61-63] also for their excited states.[42, 64-67] In the longer Ru-xy-PhOH dyad, such electrostatic effects are expected to play a smaller role, and the reaction pathway involving PCET followed by Ru(I)-to-phenoxyl electron transfer seems therefore more likely, but we are unable to observe Ru(I) or phenoxyl intermediates. However, we will show below that the activation energies associated with the photoreactions in the Ru-PhOH and Ru-xy-PhOH dyads differ by an order of magnitude which supports the hypothesis that the two dyads react through different pathways to the Ru(II) / phenolate photoproducts. Based on this hypothesis we first focus on a kinetic analysis of the photoreactions in Ru-PhOH and Ru-xy-PhOH.

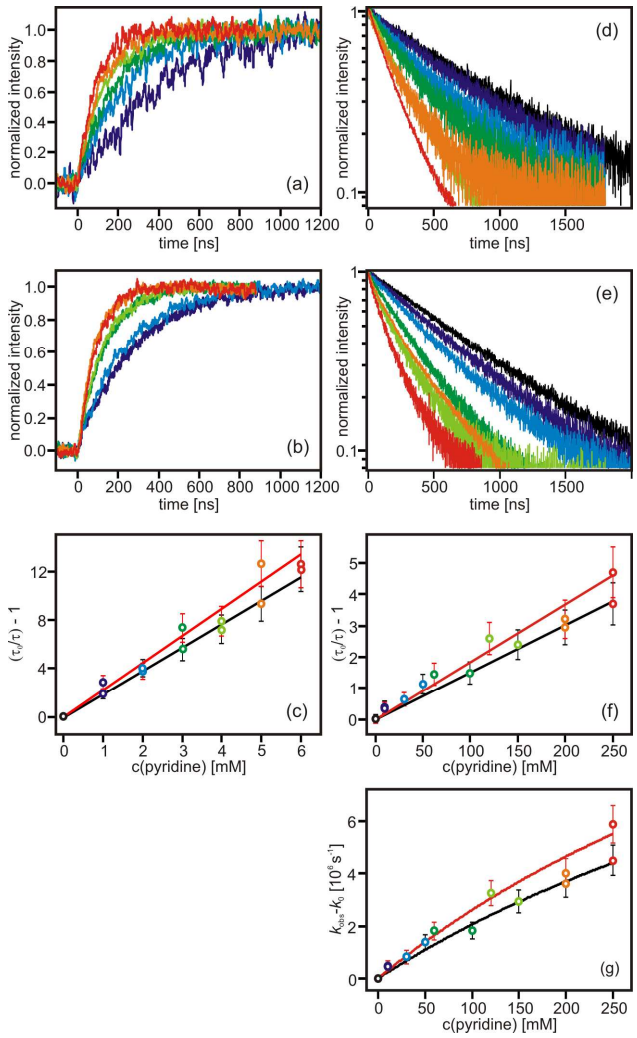

Figure 5. Rise of the transient absorption signal of Ru–PhOH (a) and Ru–PhOD (b) at 655 nm in presence of pyridine concentrations ranging from 1 to 6 mM; (c) Stern-Volmer plots based on the data from (a) and (b). The linear regression fits were forced to have intercepts of 0; their slopes correspond to the $K_{SV,H}$ and $K_{SV,D}$ values in Table 2. Luminescence decays in Ru–xy–PhOH (d) and Ru–xy–PhOD (e) at 600 nm in presence of pyridine concentrations ranging from 0 mM to 250 mM; (f) Stern-Volmer plots based on the data from (d) and (e). The linear regression fits were forced to have intercepts of 0; their slopes correspond to the $K_{SV,H}$ and $K_{SV,D}$ values in Table 2. (g) Plots of excited-state decay rate constants versus pyridine concentration for Ru-xy-PhOH and Ru-xy-PhOD with fits of eq. 2 to the experimental data as described in the text.

Figure 5a/5b shows the temporal evolution of the transient absorption signal at 655 nm as a function of time for Ru–PhOH (a) and Ru-PhOD (b). (Deuteration of the complexes occurred by repeated dissolution in CH_3CN/D_2O mixture and drying in vacuo). Analysis of these two sets of data (Figure 5c) yields Stern-Volmer constants of $K_{SV,H}$ = 1921±37 M^{-1} and $K_{SV,D}$ = 2224±98 M^{-1} for Ru–PhOH and Ru-PhOD, respectively (Table 2). Using a lifetime of 1168 ns for the $Ru(bpy)_3^{2+}$ unit of this dyad in pure CH_2Cl_2, one obtains rate constants for bimolecular excited-state quenching of $k_H = (1.7\pm0.2)\cdot10^9$ M^{-1} s^{-1} and $k_D = (2.0\pm0.2)\cdot10^9$ M^{-1} s^{-1} (Table 2).

In the Ru–xy–PhOH dyad excited-state quenching following pyridine addition is markedly less efficient than in Ru–PhOH, and we have found it most convenient to perform a Stern-Volmer analysis based on the luminescence lifetime data presented in Figure 5d/5e. The emission decays were measured at 600 nm after ~10-ns pulsed excitation at 532 nm, using normal Ru–xy–PhOH (d) and its deuterated analogue (e). The Stern-Volmer plot in Figure 5f yields $K_{SV,H}$ = 15.1±0.5 M^{-1} and $K_{SV,D}$ = 18.4±0.8 M^{-1} (Table 2).

Table 2. Kinetic parameters for the two dyads and excited-state quenching by pyridine.

		τ_0 [ns] [a]	$K_{SV,X}$ [M^{-1}] [b]	k_X [M^{-1} s^{-1}] [c]	KIE = k_H/k_D
Ru-PhOX;	X = H	1168	1921±37	$(1.7\pm0.2)\cdot10^9$	0.8±0.2
	X = D		2224±98	$(2.0\pm0.2)\cdot10^9$	
Ru-xy-PhOX;	X = H	818	15.1±0.5	$(1.9\pm0.2)\cdot10^7$	0.8±0.2
	X = D		18.4±0.8	$(2.3\pm0.3)\cdot10^7$	

[a] ^{3}MLCT lifetime in de-oxygenated CH_2Cl_2 at 293 K. [b] Stern-Volmer constants corresponding to the slopes of linear regression fits to the data in Figure 5c/5f (forced to have intercepts of 0). [c] Rate constants for bimolecular excited-state quenching were calculated using the relation $k_X = K_{SV,X} / \tau_0$.

The ^{3}MLCT lifetime of Ru–xy–PhOH in absence of pyridine is 818 ns, and this leads to $k_H = (1.9\pm0.2)\cdot10^7$ M^{-1} s^{-1} and $k_D = (2.3\pm0.3)\cdot10^7$ M^{-1} s^{-1}, which is roughly a factor of 100 lower than what has been determined for the shorter dyad (Table 2). We note that all experimental emission decays of Ru-xy-

PhOH exhibited both a fast and a slow decay component (the deviation from single exponential decay behavior is readily visible in Figure 5d/5e). We attribute the slow decay component to impurities of $Ru(bpy)_3^{2+}$ the luminescence of which is essentially unaffected by pyridine addition (at least in the concentration range used here). In our biexponential fits we fixed the slow component to 786 ns, which is what we have measured for the luminescence lifetime of $Ru(bpy)_3^{2+}$ in de-oxygenated CH_2Cl_2 at room temperature. The fast decay components arise due excited-state quenching by a photochemical reaction. As discussed above, our hypothesis is that Ru-xy-PhOH reacts through a sequence of PCET and ET reactions. The initial PCET process forming Ru(I) and phenoxyl intermediates is considered rate-determining, the ensuing Ru(I)-to-phenoxyl radical is likely to be very rapid for reasons mentioned above.

A key problem with the foregoing Stern-Volmer analysis is that it does not take into account the hydrogen-bonding equilibrium between the phenol and pyridine in CH_2Cl_2. We address this shortcoming for the Ru-xy-PhOH dyad with Figure 5g which shows a plot of $k_{obs} - k_0$ versus the pyridine concentration and make a fit to the experimental data with eq. 2;[40] k_{obs} is the inverse of τ at a given pyridine concentration, k_0 is the excited-state decay rate constant in absence of pyridine. [B] is the pyridine concentration, and K_A is the association constant for the formation of hydrogen-bonded phenol-pyridine adducts. k_{PCET} is the rate constant for intramolecular phenol-to-ruthenium electron transfer occurring in concert with release of the phenolic proton to the hydrogen-bonded pyridine.

$$k_{obs} - k_0 = k_{PCET} \cdot (K_A \cdot [B]) / (1 + K_A \cdot [B]) \quad \text{(eq. 2)}$$

This is a simplified version of an equation used recently in a very similar context;[21] the simple form of eq. 2 is due to the absence of significant direct excited-state quenching by pyridine and the fact that intramolecular electron transfer is negligible in the absence of pyridine. We have attempted to determine the association constants in an independent manner, using a luminescence-intensity based method described previously.[43] This analysis (Figure S3) yields $K_A = 1695 \pm 172$ M^{-1} for Ru-PhOH and 14.2±1.3

M^{-1} for Ru-xy-PhOH. It is impossible to reconcile these K_A values with fits of eq. 2 to the experimental data in Figure 5g using k_{PCET} as a sole fit parameter; K_A values on the order of 10 M^{-1} or greater will lead to significant curvature in the calculated plots of $k_{obs} - k_0$. What is more, the K_A value of 1695±172 M^{-1} seems far too large in comparison to other phenol-pyridine adducts in solvents of comparable polarity.[40, 68] We therefore decided to let both k_{PCET} and K_A vary freely in our fits to the data in Figure 5g, but this procedure naturally leads to large error bars. We find $k_{PCET} = (1.8\pm1.0)\cdot10^7$ s^{-1} / $K_A = 1.2\pm0.8$ M^{-1} for Ru-xy-PhOH and $k_{PCET} = (2.1\pm1.4)\cdot10^7$ s^{-1} / $K_A = 1.4\pm1.2$ M^{-1} for Ru-xy-PhOD. Evidently, we can only make order-of-magnitude estimates for k_{PCET} and K_A using this method.

H/D kinetic isotope effects and activation energies. In room temperature solution essentially no H/D kinetic isotope effects (KIEs) are observed in the data from Figure 5 even though proton motion is likely to be involved in the deactivation processes of both dyads (Table 2): In both cases we find k_H/k_D = 0.8±0.2. However, in the course of determining the activation energies for the photoreactions of the two dyads we found that the shorter one exhibits a temperature dependent H/D KIE because for Ru-PhOD the activation energy is 3 times larger than for Ru-PhOH:

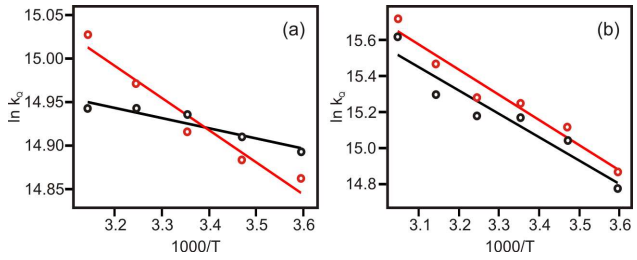

Figure 6. Arrhenius plots based on the rate constants for formation of the photoproducts obtained after pulsed excitation of (a) Ru–PhOH/D in CH_2Cl_2 with 2 mM pyridine (experimental observable: luminescence decay detected at 600 nm) and (b) Ru–xy–PhOH/D in CH_2Cl_2 with 200 mM pyridine (experimental observable: luminescence decay detected at 600 nm). Black circles: normal samples; red circles: deuterated samples. The solid lines are linear regression fits from the slopes of which the activation energies (E_A) in Table 3 were calculated.

Table 3. Activation energies (E_A) for the photoreactions of the two dyads.

	E_A (X = H) [eV]	E_A (X = D) [eV]
Ru–PhOX	0.010±0.002	0.032±0.004
Ru–xy–PhOX	0.112±0.017	0.121±0.014

The Arrhenius plot in Figure 6a shows the rates for formation of Ru(II)-PhO$^-$ after photoexcitation of Ru–PhOH (black circles) and Ru-PhOD (red circles) in 1,2-dichloroethane in presence of 2 mM pyridine; the individual data points were obtained from emission decay measurements (Figure S4), and the lifetimes extracted from these data are in good agreement with the risetimes observed for the transient absorption signal at 655 nm (data not shown). Linear regression yields an activation energy (E_A) of 0.010±0.002 eV for Ru–PhOH, whereas E_A = 0.032±0.004 eV for Ru-PhOD (Table 3).

For the Ru–xy–PhOH dyad (Figure 6b) we determine activation energies which are much more similar for proteo- and deutero-analogues: Using emission lifetimes as an experimental observable and a pyridine concentration of 200 mM in 1,2-dichloroethane (Figure S4) we determine E_A = 0.112±0.017 eV for Ru–xy–PhOH and E_A = 0.121±0.014 eV for Ru–xy–PhOD (Table 3). The factor of 10 increase of E_A between Ru–xy–PhOH and Ru–PhOH supports the hypothesis that the two dyads react via different pathways to the Ru(II) / phenolate photoproducts. The factor of 3 increase of E_A between Ru–PhOH and Ru-PhOD possibly reflects the lower zero-point energy of the O–D vibration with respect to the O–H vibration. The association constant for formation of hydrogen-bonded phenol-pyridine adducts is temperature-dependent; however, we expect that this hydrogen-bonding equilibrium is similarly influenced by temperature in all dyads considered here.

Thermal backward reactions with inverse H/D kinetic isotope effects. The transient absorption intensities at 655 nm in the shorter dyad and at 395 nm in the longer dyad exhibit single exponential

decays which, in the 2 mM – 200 mM pyridine concentration range, are essentially independent of the exact amount of pyridine present. Under these conditions the concentration of pyridinium ions seems to determine the rate for reaction of the deprotonated phenols back to their initial forms. The pyridinium concentration in turn is limited by the number of dyads which have undergone photochemical reaction, and this concentration is always lower than 10^{-5} M. In de-oxygenated CH_2Cl_2 in presence of pyridine the average decay time of the transient absorption signal at 655 nm (Figure 5a) is 50.9 μs when using Ru–PhOH and 34.2 μs when using Ru-PhOD (Table 4). Representative decay curves (obtained at a pyridine concentration of 3 mM) are shown in Figure S5a of the Supporting Information. In de-oxygenated CH_2Cl_2 in presence of up to 200 mM pyridine the transient absorption intensity at 395 nm (Figure 5c) has an average lifetime of 31.9 μs when using Ru–xy–PhOH and an average lifetime of 19.1 μs when using Ru–xy–PhOD (Table 4). Representative decay curves for the longer dyad are shown in Figure S5b. The occurrence of inverse H/D kinetic isotope effects of 0.7±0.1 for Ru-PhOH and 0.6±0.1 for Ru-xy-PhOH is rather unusual but at present the origin of this phenomenon is not clear.

Table 4. Time constants and kinetic isotope effects for thermal back reaction.

	τ_{BR} (X = H) [μs]	τ_{BR} (X = D) [μs]	KIE
Ru-PhOX	50.9	34.2	0.7±0.1
Ru-xy-PhOX	31.9	19.1	0.6±0.1

In a previously investigated rhenium(I)-phenol dyad (Re-PhOH) we had also observed a phenolate species as a major photoproduct (in CH_3CN/H_2O), while for a rhenium(I)-xylene-phenol dyad (Re-xy-PhOH) the spectroscopic data was consistent with a PCET reaction leading to a reduced rhenium complex and a phenoxyl radical.[30] Interestingly, the PCET phenoxyl radical photoproduct is much shorter-lived (85 ns) than the phenolate photoproducts observed for Ru-PhOH (50.9 μs), Ru-xy-PhOH (31.9 μs), and Re-xy-PhOH (14 μs). It thus seems that phenolate protonation in these dyads occurs

significantly more slowly than the (thermal) PCET reaction leading to disappearance of the phenoxyl radical in Re-xy-PhOH.

SUMMARY AND CONCLUSION

In pure CH_2Cl_2 none of the two dyads exhibits any photochemistry, neither electron transfer nor proton transfer nor PCET. When pyridine is present, selective excitation of their $Ru(bpy)_3^{2+}$ moieties leads to photoproducts containing Ru(II) in the ground state and a phenolate moiety. In principle, phenol deprotonation can occur via two different reaction mechanisms: (i) direct proton release from the excited dyad or (ii) initial rate-determining PCET forming Ru(I) and phenoxyl intermediates followed by rapid (because highly exergonic) phenoxyl-to-Ru(I) electron transfer. Photoacid behavior seems plausible for Ru-PhOH because of the short ruthenium – phenol distance but is less likely in the longer Ru-xy-PhOH dyad. The observation of activation energies which differ by an order of magnitude for the photochemical reactions of Ru-PhOH and Ru-xy-PhOH supports the hypothesis that the two dyads react through different reaction pathways.

The present study illustrates one of the key difficulties that can be associated with the observation of intramolecular photoinduced PCET: Initial excited-state PCET can be followed by rapid (thermal) electron transfer in the reverse direction, thereby impeding the observation of PCET photoproducts. In practice it then becomes challenging to distinguish such a reaction sequence from simple photoacid behavior.

EXPERIMENTAL SECTION

UV-Vis spectra were recorded on a Cary 300 instrument from Varian, steady-state luminescence was measured on a Fluorolog-3 instrument from Horiba Jobin-Yvon using a TBC-07C photomultiplier from Hamamatsu. Transient absorption and time-resolved emission was measured on the LP920-KS flash photolysis system from Edinburgh Instruments employing an iCCD camera from Andor and an R928 photomultiplier for detection. The laser excitation source was a frequency-doubled Quantel Brilliant b laser. Temperature control in the activation energy experiments occurred with a TC-125 instrument from Quantum Northwest. For cyclic voltammetry a Versastat3-200 potentiostat from Princeton Applied Research was employed, using a Pt disk working electrode and two silver wires as quasi-reference and counter-electrodes. Synthetic protocols and product characterization data are given in the Supporting Information. For product characterization we used the NMR, mass spectrometry, and elemental analysis equipment described previously.[30, 54] Errors reported for rate constants and KIEs are standard deviations, as obtained from corresponding fits and based on the experience that our kinetic measurements are accurate to ±10%.

ACKNOWLEDGMENT

Funding from the Deutsche Forschungsgemeinschaft (DFG) through IRTG-1422 is gratefully acknowledged.

SUPPORTING INFORMATION PARAGRAPH

Detailed synthetic protocols and product characterization data, additional electrochemical, luminescence and transient absorption data. This material is available free of charge via the Internet at http://pubs.acs.org.

REFERENCES

(1) Meyer, T. J.; Huynh, M. H. V.; Thorp, H. H. The possible role of proton-coupled electron transfer (PCET) in water oxidation by photosystem II. *Angew. Chem. Int. Ed.* **2007,** *46*, 5284-5304.

(2) Meyer, T. J. Chemical approaches to artificial photosynthesis. *Acc. Chem. Res.* **1989,** *22*, 163-170.

(3) Bordwell, F. G.; Cheng, J. P. Substituent effects on the stabilities of phenoxyl radicals and the acidities of phenoxyl radical cations. *J. Am. Chem. Soc.* **1991,** *113*, 1736-1743.

(4) Warren, J. J.; Tronic, T. A.; Mayer, J. M. Thermochemistry of Proton-Coupled Electron Transfer Reagents and its Implications. *Chem. Rev.* **2010,** *110*, 6961-7001.

(5) Mayer, J. M. Proton-coupled electron transfer: A reaction chemist's view. *Annu. Rev. Phys. Chem.* **2004,** *55*, 363-390.

(6) Roth, J. P.; Yoder, J. C.; Won, T. J.; Mayer, J. M. Application of the Marcus cross relation to hydrogen atom transfer reactions. *Science* **2001,** *294*, 2524-2526.

(7) Reece, S. Y.; Nocera, D. G. Proton-Coupled Electron Transfer in Biology: Results from Synergistic Studies in Natural and Model Systems. *Annu. Rev. Biochem.* **2009,** *78*, 673-699.

(8) Costentin, C.; Robert, M.; Savéant, J.-M. Concerted Proton-Electron Transfers: Electrochemical and Related Approaches. *Acc. Chem. Res.* **2010,** *43*, 1019-1029.

(9) Maki, T.; Araki, Y.; Ishida, Y.; Onomura, O.; Matsumura, Y. Construction of persistent phenoxyl radical with intramolecular hydrogen bonding. *J. Am. Chem. Soc.* **2001,** *123*, 3371-3372.

(10) Markle, T. F.; Mayer, J. M. Concerted proton-electron transfer in pyridylphenols: The importance of the hydrogen bond. *Angew. Chem. Int. Ed.* **2008,** *47*, 738-740.

(11) Rhile, I. J.; Markle, T. F.; Nagao, H.; DiPasquale, A. G.; Lam, O. P.; Lockwood, M. A.; Rotter, K.; Mayer, J. M. Concerted proton-electron transfer in the oxidation of hydrogen-bonded phenols. *J. Am. Chem. Soc.* **2006,** *128*, 6075-6088.

(12) Rhile, I. J.; Mayer, J. M. One-electron oxidation of a hydrogen-bonded phenol occurs by concerted proton-coupled electron transfer. *J. Am. Chem. Soc.* **2004,** *126*, 12718-12719.

(13) Markle, T. F.; Tenderholt, A. L.; Mayer, J. M. Probing Quantum and Dynamic Effects in Concerted Proton-Electron Transfer Reactions of Phenol-Base Compounds. *J. Phys. Chem. B* **2012,** *116*, 571-584.

(14) Markle, T. F.; Rhile, I. J.; DiPasquale, A. G.; Mayer, J. M. Probing concerted proton-electron transfer in phenol-imidazoles. *Proc. Natl. Acad. Sci. U. S. A.* **2008,** *105*, 8185-8190.

(15) Irebo, T.; Johansson, O.; Hammarström, L. The rate ladder of proton-coupled tyrosine oxidation in water: A systematic dependence on hydrogen bonds and protonation state. *J. Am. Chem. Soc.* **2008,** *130*, 9194-9195.

(16) Sjödin, M.; Irebo, T.; Utas, J. E.; Lind, J.; Merenyi, G.; Åkermark, B.; Hammarström, L. Kinetic effects of hydrogen bonds on proton-coupled electron transfer from phenols. *J. Am. Chem. Soc.* **2006,** *128*, 13076-13083.

(17) Schrauben, J. N.; Cattaneo, M.; Day, T. C.; Tenderholt, A. L.; Mayer, J. M. Mutiple-Site Concerted Proton-Electron Transfer REactions of Hydrogen-Bonded Phenols are Nonadiabatic and Well Described by Semiclassical Marcus Theory. *J. Am. Chem. Soc.* **2012,** *134*, 16635–16645.

(18) Costentin, C.; Robert, M.; Savéant, J. M.; Tard, C. Inserting a Hydrogen-Bond Relay between Proton Exchanging Sites in Proton-Coupled Electron Transfers. *Angew. Chem. Int. Ed.* **2010,** *49*, 3803-3806.

(19) Costentin, C.; Robert, M.; Savéant, J. M.; Tard, C. H-bond relays in proton-coupled electron transfers. Oxidation of a phenol concerted with proton transport to a distal base through an OH relay. *Phys. Chem. Chem. Phys.* **2011,** *13*, 5353-5358.

(20) Benisvy, L.; Bittl, R.; Bothe, E.; Garner, C. D.; McMaster, J.; Ross, S.; Teutloff, C.; Neese, F. Phenoxyl radicals hydrogen-bonded to imidazolium: Analogues of tyrosyl D of photosystem II: High-field EPR and DFT studies. *Angew. Chem. Int. Ed.* **2005,** *44*, 5314-5317.

(21) Pizano, A. A.; Yang, J. L.; Nocera, D. G. Photochemical tyrosine oxidation with a hydrogen-bonded proton acceptor by bidirectional proton-coupled electron transfer. *Chem. Sci.* **2012,** *3*, 2457-2461.

(22) Zhang, M.-T.; Irebo, T.; Johansson, O.; Hammarström, L. Proton-Coupled Electron Transfer from Tyrosine: A Strong Rate Dependence on Intramolecular Proton Transfer Distance. *J. Am. Chem. Soc.* **2011,** *133*, 13224-13227.

(23) Markle, T. F.; Rhile, I. J.; Mayer, J. M. Kinetic Effects of Increased Proton Transfer Distance on Proton-Coupled Oxidations of Phenol-Amines. *J. Am. Chem. Soc.* **2011,** *133*, 17341-17352.

(24) Irebo, T.; Reece, S. Y.; Sjödin, M.; Nocera, D. G.; Hammarström, L. Proton-coupled electron transfer of tyrosine oxidation: Buffer dependence and parallel mechanisms. *J. Am. Chem. Soc.* **2007,** *129*, 15462-15464.

(25) Irebo, T.; Zhang, M.-T.; Markle, T. F.; Scott, A. M.; Hammarström, L. Spanning Four Mechanistic Regions of Intramolecular Proton-Coupled Electron Transfer in a $Ru(bpy)_3^{2+}$-Tyrosine Complex. *J. Am. Chem. Soc.* **2012,** *134*, 16247–16254.

(26) Costentin, C.; Robert, M.; Savéant, J. M. Concerted proton-electron transfer reactions in water. Are the driving force and rate constant depending on pH when water acts as proton donor or acceptor? *J. Am. Chem. Soc.* **2007,** *129*, 5870-5879.

(27) Bonin, J.; Costentin, C.; Louault, C.; Robert, M.; Savéant, J. M. Water (in Water) as an Intrinsically Efficient Proton Acceptor in Concerted Proton Electron Transfers. *J. Am. Chem. Soc.* **2011,** *133*, 6668-6674.

(28) Manner, V. W.; DiPasquale, A. G.; Mayer, J. M. Facile concerted proton-electron transfers in a ruthenium terpyridine-4'-carboxyl ate complex with a long distance between the redox and basic sites. *J. Am. Chem. Soc.* **2008,** *130*, 7210-7211.

(29) Manner, V. W.; Mayer, J. M. Concerted Proton-Electron Transfer in a Ruthenium Terpyridyl-Benzoate System with a Large Separation between the Redox and Basic Sites. *J. Am. Chem. Soc.* **2009,** *131*, 9874-9875.

(30) Kuss-Petermann, M.; Wolf, H.; Stalke, D.; Wenger, O. S. Influence of Donor-Acceptor Distance Variation on Photoinduced Electron and Proton Transfer in Rhenium(I)-Phenol Dyads. *J. Am. Chem. Soc.* **2012,** *134*, 12844-12854.

(31) Warren, J. J.; Menzeleev, A. R.; Kretchmer, J. S.; Miller, T. F.; Gray, H. B.; Mayer, J. M. Long-Range Proton-Coupled Electron-Transfer Reactions of Bis(imidazole) Iron Tetraphenylporphyrins Linked to Benzoates. *J. Phys. Chem. Lett.* **2013,** *4*, 519-523.

(32) Edwards, P. P.; Gray, H. B.; Lodge, M. T. J.; Williams, R. J. P. Electron transfer and electronic conduction through an intervening medium. *Angew. Chem. Int. Ed.* **2008,** *47*, 6758-6765.

(33) Gray, H. B.; Winkler, J. R. Long-range electron transfer. *Proc. Natl. Acad. Sci. U. S. A.* **2005,** *102*, 3534-3539.

(34) Eng, M. P.; Albinsson, B. Non-exponential distance dependence of bridge-mediated electronic coupling. *Angew. Chem. Int. Ed.* **2006,** *45*, 5626-5629.

(35) Weiss, E. A.; Ahrens, M. J.; Sinks, L. E.; Gusev, A. V.; Ratner, M. A.; Wasielewski, M. R. Making a molecular wire: Charge and spin transport through para-phenylene oligomers. *J. Am. Chem. Soc.* **2004,** *126*, 5577-5584.

(36) Wenger, O. S. How Donor-Bridge-Acceptor Energetics Influence Electron Tunneling Dynamics and Their Distance Dependences. *Acc. Chem. Res.* **2011,** *44*, 25-35.

(37) Indelli, M. T.; Chiorboli, C.; Flamigni, L.; De Cola, L.; Scandola, F. Photoinduced electron transfer across oligo-*p*-phenylene bridges. Distance and conformational effects in Ru(II)-Rh(III) dyads. *Inorg. Chem.* **2007,** *46*, 5630-5641.

(38) Costentin, C.; Robert, M.; Savéant, J. M. Electrochemical and homogeneous proton-coupled electron transfers: Concerted pathways in the one-electron oxidation of a phenol coupled with an intramolecular amine-driven proton transfer. *J. Am. Chem. Soc.* **2006,** *128*, 4552-4553.

(39) Costentin, C.; Robert, M.; Savéant, J. M. Concerted proton-electron transfers in the oxidation of phenols. *Phys. Chem. Chem. Phys.* **2010,** *12*, 11179-11190.

(40) Biczok, L.; Gupta, N.; Linschitz, H. Coupled electron-proton transfer in interactions of triplet C-60 with hydrogen-bonded phenols: Effects of solvation, deuteration, and redox potentials. *J. Am. Chem. Soc.* **1997,** *119*, 12601-12609.

(41) Gagliardi, C. J.; Westlake, B. C.; Kent, C. A.; Paul, J. J.; Papanikolas, J. M.; Meyer, T. J. Integrating proton coupled electron transfer (PCET) and excited states. *Coord. Chem. Rev.* **2010,** *254*, 2459-2471.

(42) Wenger, O. S. Proton-Coupled Electron Transfer Originating from Excited States of Luminescent Transition-Metal Complexes. *Chem.-Eur. J.* **2011,** *17*, 11692-11702.

(43) Concepcion, J. J.; Brennaman, M. K.; Deyton, J. R.; Lebedeva, N. V.; Forbes, M. D. E.; Papanikolas, J. M.; Meyer, T. J. Excited-state quenching by proton-coupled electron transfer. *J. Am. Chem. Soc.* **2007,** *129*, 6968-6969.

(44) Moore, G. F.; Hambourger, M.; Gervaldo, M.; Poluektov, O. G.; Rajh, T.; Gust, D.; Moore, T. A.; Moore, A. L. A bioinspired construct that mimics the proton coupled electron transfer between $P680^{\bullet+}$ and the Tyr_z-His_{190} pair of photosystem II. *J. Am. Chem. Soc.* **2008,** *130*, 10466-10467.

(45) Bronner, C.; Wenger, O. S. Proton-Coupled Electron Transfer between 4-Cyanophenol and Photoexcited Rhenium(I) Complexes with Different Protonatable Sites. *Inorg. Chem.* **2012,** *51*, 8275-8283.

(46) Bronner, C.; Wenger, O. S. Kinetic Isotope Effects in Reductive Excited-State Quenching of Ru(2,2 '-bipyrazine)$_3^{2+}$ by Phenols. *J. Phys. Chem. Lett.* **2012,** *3*, 70-74.

(47) Wenger, O. S. Proton-Coupled Electron Transfer with Photoexcited Metal Complexes. *Acc. Chem. Res.* **2013**, doi: 10.1021/ar300289x.

(48) Renger, G.; Renger, T. Photosystem II: The machinery of photosynthetic water splitting. *Photosynth. Res.* **2008,** *98*, 53-80.

(49) Magnuson, A.; Berglund, H.; Korall, P.; Hammarström, L.; Åkermark, B.; Styring, S.; Sun, L. C. Mimicking electron transfer reactions in photosystem II: Synthesis and photochemical characterization of a ruthenium(II) tris(bipyridyl) complex with a covalently linked tyrosine. *J. Am. Chem. Soc.* **1997,** *119*, 10720-10725.

(50) Lachaud, T.; Quaranta, A.; Pellegrin, Y.; Dorlet, P.; Charlot, M. F.; Un, S.; Leibl, W.; Aukauloo, A. A biomimetic model of the electron transfer between P-680 and the Tyr_Z-His_{190} pair of PSII. *Angew. Chem. Int. Ed.* **2005,** *44*, 1536-1540.

(51) Sun, L. C.; Burkitt, M.; Tamm, M.; Raymond, M. K.; Abrahamsson, M.; LeGourriérec, D.; Frapart, Y.; Magnuson, A.; Kenéz, P. H.; Brandt, P.; Tran, A.; Hammarström, L.; Styring, S.; Åkermark, B. Hydrogen-bond promoted intramolecular electron transfer to photogenerated Ru(III): A functional mimic of Tyrosine(Z) and histidine 190 in photosystem II. *J. Am. Chem. Soc.* **1999,** *121*, 6834-6842.

(52) Sjödin, M.; Styring, S.; Åkermark, B.; Sun, L. C.; Hammarström, L. Proton-coupled electron transfer from tyrosine in a tyrosine-ruthenium-tris-bipyridine complex: Comparison with Tyrosine(z) oxidation in photosystem II. *J. Am. Chem. Soc.* **2000,** *122*, 3932-3936.

(53) Johansson, O.; Wolpher, H.; Borgström, M.; Hammarström, L.; Bergquist, J.; Sun, L. C.; Åkermark, B. Intramolecular charge separation in a hydrogen bonded tyrosine-ruthenium(II)-naphthalene diimide triad. *Chem. Commun.* **2004**, 194-195.

(54) Hankache, J.; Niemi, M.; Lemmetyinen, H.; Wenger, O. S. Photoinduced Electron Transfer in Linear Triarylamine-Photosensitizer-Anthraquinone Triads with Ruthenium(II), Osmium(II), and Iridium(III). *Inorg. Chem.* **2012,** *51*, 6333-6344.

(55) Cargill Thompson, A. M. W.; Smailes, M. C. C.; Jeffery, J. C.; Ward, M. D. Ruthenium tris-(bipyridyl) complexes with pendant protonatable and deprotonatable moieties: pH sensitivity of electronic spectral and luminescence properties. *J. Chem. Soc., Dalton Trans.* **1997**, 737-743.

(56) Milder, S. J.; Gold, J. S.; Kliger, D. S. Temperature-dependence of the excited-state absorption of $Ru(bpy)_3^{2+}$. *J. Phys. Chem.* **1986,** *90*, 548-550.

(57) Weller, A. Photoinduced electron-transfer in solution - Exciplex and radical ion-pair formation free enthalpies and their solvent dependence. *Z. Phys. Chem.* **1982,** *133*, 93-98.

(58) Heath, G. A.; Yellowlees, L. J.; Braterman, P. S. Spectro-electrochemical studies on tris-bipyridyl ruthenium complexes - UV, visible, and near-infrared spectra of the series $Ru(bipyridyl)_3^{2+/1+/0/1-}$. *J. Chem. Soc., Chem. Commun.* **1981**, 287-289.

(59) Lomoth, R.; Haupl, T.; Johansson, O.; Hammarström, L. Redox-switchable direction of photoinduced electron transfer in an $Ru(bpy)_3^{2+}$-Viologen dyad. *Chem.-Eur. J.* **2002,** *8*, 102-110.

(60) Hanss, D.; Wenger, O. S. Conformational effects on long-range electron transfer: Comparison of oligo-*p*-phenylene and oligo-*p*-xylene bridges. *Eur. J. Inorg. Chem.* **2009**, 3778-3790.

(61) Carina, R. F.; Verzegnassi, L.; Bernardinelli, G.; Williams, A. F. Modulation of iron reduction potential by deprotonation at a remote site. *Chem. Commun.* **1998**, 2681-2682.

(62) Jones, H.; Newell, M.; Metcalfe, C.; Spey, S. E.; Adams, H.; Thomas, J. A. Deprotonation of a ruthenium(II) complex incorporating a bipyrazole ligand leading to optical and electrochemical switching. *Inorg. Chem. Commun.* **2001,** *4*, 475-477.

(63) Klein, S.; Dougherty, W. G.; Kassel, W. S.; Dudley, T. J.; Paul, J. J. Structural, Electronic, and Acid/Base Properties of $Ru(bpy)_2(bpy(OH)_2)^{2+}$ (bpy=2,2 '-Bipyridine, $bpy(OH)_2$=4,4 '-Dihydroxy-2,2 '-bipyridine). *Inorg. Chem.* **2011,** *50*, 2754-2763.

(64) Vos, J. G. Excited-state acid-base properties of inorganic compounds. *Polyhedron* **1992,** *11*, 2285-2299.

(65) Sun, H.; Hoffman, M. Z. Protonation of the excited-states of ruthenium(II) complexes containing 2,2'-bipyridine, 2,2'-bipyrazine,and 2,2'-bipyrimidine ligands in aqueous solution. *J. Phys. Chem.* **1993,** *97*, 5014-5018.

(66) Giordano, P. J.; Bock, C. R.; Wrighton, M. S.; Interrante, L. V.; Williams, R. F. X. Excited-state proton-transfer of a metal-complex - Determination of acid dissociation-constant for a metal-to-ligand charge-transfer state of a ruthenium(II) complex. *J. Am. Chem. Soc.* **1977,** *99*, 3187-3189.

(67) Bare, W. D.; Mack, N. H.; Demas, J. N.; DeGraff, B. A. pH-dependent photophysical behavior of rhenium complexes containing hydroxypyridine ligands. *Appl. Spectr.* **2004,** *58*, 1093-1100.

(68) Biczók, L.; Linschitz, H. Concerted electron and proton movement in quenching of triplet C-60 and tetracene fluorescence by hydrogen-bonded phenol-base pairs. *J. Phys. Chem.* **1995,** *99*, 1843-1845.

SYNOPSIS TOC